Simulation of photocatalytic planar microreactor for degradation of cephalexin in contaminated water

M.R. Abbasi, F. Rabanimehr, A.R. Solaimany Nazar*, and M. Farhadian

Department of Chemical Engineering, Faculty of Engineering, University of Isfahan, Isfahan, Iran.

Abstract

The degradation of pollutants in a planar continuous flow photocatalytic microreactor was simulated using COMSOL Multiphysics. The Langmuir-Hinshelwood model was proposed to describe the available experimental data for the reaction kinetics of cephalexin (CEX) degradation from aqueous solution using the Bi_2WO_6/CNT/TiO_2 photocatalyst, and the kinetic constants of this model were evaluated. The predicted results for the breakthrough curves of this pollutant at the microreactor outlet were compared with experimental data. The mean absolute error between the model and experimental values at inlet CEX concentrations of 30, 40, 50, and 60 mg/L was 3.3%, indicating a good model prediction. The parametric study results indicate that increasing the length of the microreactor from 50 to 100 mm enhances the removal efficiency from 82 to 97%. Additionally, reducing the microreactor depth from 300 to 100 μm increases the removal efficiency from 82 to 92%. The calculated Damköhler number under the optimal experimental conditions was 0.42, indicating that the photocatalytic process is primarily controlled by reaction kinetics rather than mass transfer limitations.

Keywords: planar microreactor, photocatalytic degradation, simulation, Langmuir-Hinshelwood, continuous flow

1. Introduction

Increasing water consumption to meet agricultural, industrial, and urban needs threatens global water security [1]. Antibiotics, as one of the most important medicinal compounds, are widely used in medical activities worldwide. However, antibiotics cannot be completely metabolized in human or animal bodies and are released into the environment, causing them to spread into water and soil, which poses serious health risks [2,3]. Therefore, water and wastewater treatments become essential to mitigate water scarcity. Conventional wastewater treatment processes often

fail to reduce the concentration of toxic or resistant organic substances below acceptable levels, necessitating the adoption of more effective treatment technologies [4]. Therefore, the use of heterogeneous photocatalysts, in which the reactants and catalyst exist in different phases, has gained significant attention for removing organic pollutants from water. This method can achieve mineralization of pollutants at minimal cost [5]. Among the reactors used for photocatalytic removal, microreactors have attracted considerable attention over the past two decades due to their enhanced ability to rapidly remove pollutants from water and wastewater. Microreactors offer numerous advantages, such as a high surface area to volume ratio, short molecular penetration path, uniform light distribution, and reduced reaction time compared to conventional reactors [6,7]. Computational fluid dynamics (CFD) has proven to be an efficient and cost-effective tool in engineering, particularly in the development and modeling of photocatalytic reactors. CFD considers mass transfer, momentum transfer, and reactions kinetics to accurately predict the performance of heterogeneous photocatalytic reactors [8,9]. Modeling and CFD can contribute to better design and cost reduction in water and wastewater treatment research [10,11]. Hasanpour et al. [12] investigated the degradation performance of methyl orange using a Cellulose/Zinc oxide hybrid aerogel through modeling with MATLAB and COMSOL Multiphysics software. Their results showed good agreement between the experimental data and the predicted numerical values. Numerical modeling confirmed that the CA/ZnO-0.4 case was introduced as the best case due to faster maximum degradation efficiency being achieved. Orozco et al. [13] coupled a radiative transfer model to a first-order kinetic model for estimating dye concentration decay in a batch type hydrodynamic operation with a recirculation system. They validated this model with the experimental data on the degradation of Reactive Blue 69 anthraquinone with a TiO_2 photocatalyst, showing good agreement with the experimental results. Asgharian et al. [14] studied the degradation of tetracycline using an rGO/ZnO/Cu photocatalyst in a stirred photoreactor, solving the mass transfer, momentum transfer, and reaction kinetics equations. The model predictions matched well with the experimentally measured concentrations. The study by Corbel et al. [15] focused on both experimental and computational studies of mass transfer in a microchannel photocatalytic reactor, focusing on the degradation of cephalexin (CEX) using TiO_2 nanoparticles as an immobilized photocatalyst. Their simulations agreed well with the experimental results, and they developed a correlation for Sherwood number determination that can be applied to different microchannel configurations. In another study, Jayamohan et al. [16] evaluated a planar

microreactor employing a titanium nanotube array and TiO_2 nanopowder as photocatalysts. Their investigation of methylene blue degradation revealed the superior performance of the titanium nanotube array over TiO_2 nanopowder. Simulations indicated that CEX degradation in the microreactor is not hindered by mass transfer limitations. Satuf et al. [17] developed a simple method to obtain the intrinsic kinetic constants for first-order reactions in a photocatalytic microreactor, evaluating the degradation of clofibric acid under different flow rates and radiation fluxes using a TiO_2 photocatalyst. Their results showed good agreement between the model and experimental data. Behineh et al. [18] simulated photocatalytic pollutant removal in four microreactors, with results consistent with experimental data on methylene blue removal in microcapillary reactors and dimethylformamide and salicylic acid in microchannel reactors. The Langmuir-Hinshelwood model described the kinetic rate, with parametric studies showing increased removal efficiency with greater microreactor length and decreased depth. Corbel et al. [19] investigated the photocatalytic performance of ZnO in removing ifosfamide pollutants with different initial concentrations in a spiral microreactor. By simulating the photocatalytic experiments, they calculated the Langmuir-Hinshelwood model constants and the Damköhler number, indicating mass transfer limitations. Yusuf et al. [20] studied the performance of N-TiO_2/rGO photocatalyst in the degradation of 4-nitrophenol at different initial concentrations and under simulated sunlight in a plate structure microreactor. They also designed a model for predicting laboratory results by using computational fluid dynamics using COMSOL Multiphysics, the results were in good agreement with the experimental data. Yusuf et al. [21] investigated the modeling of a photocatalytic parallel channel microreactor for the degradation of 4-nitrophenol. They examined the effects of the initial concentration of 4-nitrophenol, flow rate, and length on the degradation percentage using COMSOL Multiphysics software. The simulation results showed that changing the initial concentration affects the initial degradation rate. Increasing the flow rate reduces the percentage of degradation, and increasing the length of the channel leads to an increase in the percentage of degradation. In a study conducted by Rabanimehr et al. [22], they studied the simulation of photocatalytic degradation of methylene blue in a continuous flow planar microreactor. Their simulation was performed by COMSOL Multiphysics and the Langmuir-Hinshelwood kinetic model was considered for the photocatalytic degradation reactions. Moreover, the effects of microreactor depth and inlet flow rate on the degradation of

methylene blue were investigated and the results showed that microreactors had lower depth and flow rate will have higher efficiency.

This study is carried out on two-dimensional simulation of the photocatalytic degradation of pollutants from polluted water in a plate microreactor by COMSOL Multiphysics. The predicted pollutant concentration at each residence time is confirmed by the available experimental data on the photocatalytic degradation of CEX reported in [23]. A parametric study is conducted to investigate the effect of geometric size of the microreactor on the CEX photodegradation rate.

2. Case Study

According to our previously published research [23], the microreactor used in this study has a flat design and plate structure. As shown in Fig. 1, the microreactor consists of two stainless steel plates, one containing the reaction chamber and inlet and outlet connections, and the other containing a rectangular window to hold the glass cover. The flow rate of the contaminant solution entering the microreactor is provided and controlled by a syringe pump. The dimensional specifications of the microreactor and operating conditions are given in Table 1. A series of experiments were conducted for CEX adsorption and degradation from contaminated water using Bi_2WO_6/CNT/TiO_2 (BCT) photocatalyst in this microreactor [23]. The photocatalyst was synthesized by hydrothermal method and then loaded on chitosan nanofibers in the presence of glutaraldehyde (GA) as a cross-linking agent. To perform the photocatalytic reactions in a microreactor fixed with the BCT photocatalyst, a 20 W xenon lamp was used as a source of UV-visible light radiation, and the light reached the nanofibers containing photocatalyst from the glass window located on the upper surface of the microreactor, and photocatalytic reactions were performed. In this study, the values of density, viscosity, diffusion coefficient of CEX, surface reaction rate constant, and absorption constant are considered to be 1000 kg/m^3, 0.001 kg/m.s, 4.56×10^{-10} m^2/s [24], 0.68 mg/L.s, and 0.023 L/mg, respectively [23].

Fig. 1

Table 1

3. Simulation

3.1. Assumptions

The model incorporates several key assumptions:

- The dilution of the solution has incorporated the physical properties of water into the model framework.
- The model operates under steady-state conditions.
- The catalyst surface is considered smooth.
- The photocatalyst is coated only on the bottom surface of the microreactor channel.
- The flow within the microreactor is considered to be single-phase.
- The fluid exhibits Newtonian behavior and is considered incompressible.
- Mass transfer by convection and molecular diffusion is considered in the axial and vertical directions, respectively.
- It is assumed that there is no pollutant concentration gradient in the lateral direction of the channel where the walls are not coated with photocatalyst. Therefore, the 2D simulation has enough accuracy to obtain the results.

3.. Governing equations

The simulation of laminar flow within the microreactor utilizes the Navier-Stokes equations for momentum conservation and the continuity equations for mass conservation.

$$\vec{u}.\nabla\vec{u} = -\nabla p + \mu\nabla^2\vec{u} \quad (1)$$

$$\rho.\nabla\vec{u} = 0 \quad (2)$$

In these equations, u, ρ, μ, and p represent the velocity field of the flow, the density of the fluid, the dynamic viscosity of the fluid, and the pressure within the fluid, respectively. Additionally, the mass transfer of species within the microreactor is described using a convection-diffusion equation.

$$\nabla.\left(-D_i\nabla c_i + c_i u\right) = 0 \tag{3}$$

where, c_i is defined as the concentration of a particular species, while D_i stands for the diffusion coefficient associated with that species. Eq. (3) incorporates the assumption of a steady-state condition. Furthermore, the process of pollutant removal is characterized using the Langmuir-Hinshelwood kinetic model. This model, which combines aspects of adsorption kinetics, is widely applied in research on photocatalytic elimination of organic contaminants in water [26].

$$r_i = \frac{k_{LHa} K c_s}{1 + K c_s} \tag{4}$$

where, k_{LHa} (mol/m^2.s) is the surface reaction rate constant (5.8×10^{-7} mol/m^2.s), K (m^3/mol) is the adsorption constant (8.045 m^3/mol) and c_s is the pollutant surface concentration.

3.3. Boundary conditions

The volumetric flow rate and pollutant concentration at the inlet of the microreactor are known, and the no-slip boundary condition is applied to the channel surfaces. The gauge pressure of the fluid at the outlet of the microreactor is zero, and the concentration gradient of the pollutant at the outlet of the microreactor is zero. On the surface of the catalyst, according to the mentioned assumptions, the following conditions are considered:

$$r_i = -D_i\nabla c_s \tag{5}$$

4. Geometry and meshing

The photodegradation of the pollutant was simulated in a 2D domain using the finite element method using COMSOL Multiphysics software version 6. The computations were performed on a computer with Intel® Core™ i7-4500U CPU @ 2.40 GHz and installed memory (RAM) 6 GB. The geometry drawn in the software is given in Fig. 2. Here, the finite element method (FEM) was employed for the numerical simulation. A triangular mesh with a normal distribution of elements was utilized to discretize the computational domain.

4.1. Mesh independency analysis

Mesh independence analysis was performed for three types of grid systems with a different number of elements. The results of this analysis are given in Table 2. The accuracy of the obtained results is verified based on the available experimental data. The best network is the normal network type, with a reasonable number of elements and very accurate results compared to the available experimental data, so this type of network is chosen for research simulation.

Table 2

Fig. 2

5. Results and discussion

5.1. Validation of the proposed model

The simulations predicted the average output concentration of the CEX pollutant in the microreactor for various residence times. To evaluate the accuracy of the model, the average absolute deviation percentage (ADD%) was calculated, comparing the model predictions with the available experimental data, as outlined in Eq. (6).

$$ADD = \frac{1}{n}\sum_{i=1}^{n}\left|c_i^{calc.} - c_i^{\exp.}\right| \tag{6}$$

The pollutant degradation efficiency is defined as Eq. (7):

$$X = \left(\frac{C_0 - C_{out}}{C_0}\right)\times 100 \tag{7}$$

where, C_0 and C_{out} represent the inlet and outlet concentrations of CEX in the microreactor, respectively. Fig. 3 shows the predicted and experimental CEX concentration [23] at the outlet of the microreactor as a function of residence time under light irradiation with an intensity of 17.45 W/m^2, pH: 4 for four inlet concentrations of 30, 40, 50, and 60 mg/L. As shown in Fig. 3, there is a very good agreement between the available experimental data and the model results. Table 3 presents a comparison between the experimental data and the degradation efficiency predicted by

the model in 2D and 3D simulations under the mentioned conditions. According to Table 4, the differences between the results in these two simulated cases are from 1 to 3%. This finding supports the validity of assuming a two-dimensional approach for the simulations in this study. The AAD percent of the model in predicting the experimental results is given in Table 5. The average absolute deviation for each graph confirms the validity of the model. Moreover, according to this table, the predicted degradation efficiency of the CEX, with an average error of 3.3% compared to the experimental data, demonstrates the good accuracy of the proposed model.

Fig. 3

Table 3

Table 4

Table 5

Fig. 4 illustrates the pollutant concentration distribution in the microreactor. This representation corresponds to a residence time of 252 seconds, an inlet concentration of 29 mg/L, and a flow rate of 71 µL/min under optimal experimental conditions in which the highest degradation efficiency of CEX was achieved [23]. The figure also highlights the molecular diffusion process of the pollutant from the bulk phase to the surface of the catalyst. According to the Langmuir-Hinshelwood kinetic model, pollutant molecules are initially adsorbed onto the catalyst surface, followed by degradation.

As evident from Fig. 4, the pollutant concentration on the catalyst surface is lower compared to the bulk phase. Additionally, along the catalytic surface and the length of the microreactor, as we move away from the inlet, pollutant molecules have more opportunities to contact the catalytic surface and undergo degradation. Consequently, a greater number of pollutant molecules are affected by the photocatalytic process, leading to a thicker layer of degraded pollutants. The average output concentration during this residence time is about 0.015 mol/m^3.

Fig. 4

5.2. Parametric study

5.2.1. Effect of microreactor depth on degradation

The impact of varying the depth of the microreactor on the degradation of the CEX pollutant was explored by prediction the performance of microreactor over a range of depth values. The effect of microreactor depth on pollutant degradation at a constant flow rate is shown in Fig. 5.

As the weight hourly space velocity (WHSV) of the feed is decreased by reducing the channel depth under the condition of constant inlet velocity, the ratio of the contacted active sites of the catalyst surface to the number of pollutant molecules is increased, leading to an improvement in degradation efficiency. Moreover, a decrease in channel depth reduces the penetration length of the pollutant molecules to the catalyst surface, consequently, reducing the mass transfer resistance and increasing the pollutant degradation rate. As the microreactor depth decreases, the wall effects become more pronounced, which significantly impacts the flow characteristics and mass transfer processes. In shallow channels, the surface-to-volume ratio increases, meaning a larger fraction of the fluid is in close contact with the catalytic surface. This enhances the degradation efficiency as more reactants interact with the surface [15]. The removal rate is increased by about 10% when decreasing the microchannel depth from 300 to 100 μm.

Fig. 5

5.2.2. Effect of microreactor length on pollutant degradation

In this section, different lengths of the microreactors, including 30, 40, 50, 60, 70, 80, 90, and 100 mm, are applied in the simulation and examined their effects on pollutant degradation efficiency at a constant inlet flow rate. Fig. 6 shows the degradation efficiency as a function of microchannel length. According to Fig. 6, the pollutant degradation percentage is increased with an increase in the length of the microreactor. Longer microreactors provide longer contact times, allowing the pollutant molecules more time to interact with the catalytic surface. This increased residence time facilitates more effective collisions between the pollutant and the catalyst, thereby enhancing the degradation efficiency. For instance, the removal efficiency of CEX was increased from 82 to 97%

as the microreactor length was increased from 50 to 100 mm, with a volumetric flow rate of 1.1905×10^{-9} m^3/s and at inlet CEX concentration of 29 mg/L.

Fig. 6

Damköhler number expresses the ratio of the chemical reaction rate to diffusion mass transfer rate. It can be used to determine whether reaction kinetics or mass transfer is the limiting control in a microreactor. When Damköhler number is less than 1, mass transfer limitations are not considered, but when the value of this number is greater than 1, the system is considered to have mass transfer limitations. For photocatalytic reactions that follow Langmuir-Hinshelwood kinetics, Damköhler number is defined as Eq. (8) [28]:

$$Da = \frac{k_{LHa}}{\frac{k_m \alpha}{K} + k_m \alpha c_0} \tag{8}$$

In this relation, α, C_0, and k_m represent the surface-to-volume ratio of the microreactor (3330 m^{-1}), the inlet concentration of CEX, and the mass transfer coefficient in m/s, respectively. To determine Damköhler number, it is first necessary to determine the value of the mass transfer coefficient. Ergu et al. [28] have presented Eq. (9) to determine the mass transfer coefficient in microreactors with a rectangular cross-section.

$$Sh = \frac{k_m d_h}{D} = 2.76\times \mathrm{Re}^{0.28}\left(\frac{L}{d_h}\right)^{-0.12}\times Sc^{1/3} \qquad 0.1<\mathrm{Re}<1 \tag{9}$$

In the above relation, the factors Sh, k_m, d_h, D, Re, Sc, and L, respectively, express the dimensionless Sherwood number, the hydraulic diameter in m, the diffusion coefficient of CEX in m^2/s, the dimensionless Reynolds number, the dimensionless Schmidt number, and the length of the microreactor is in m.

The value of Damköhler number at the inlet concentration of 29 mg/L is calculated for different flow rates, and a plot of Damköhler number in terms of the Reynolds number is shown in Fig. 7. According to Fig. 7, Damköhler number is less than one at different flow rates, indicating that there is no mass transfer limitation in the fluid. The lack of mass transfer limitation is due to the low depth of the microreactor and the short length of the pollutant penetration path.

Fig. 7

5.3. Experimental insights into adsorption and degradation mechanisms

Fig. 8 illustrates the potential interactions between chitosan and CEX observed in the adsorption-photocatalytic experiments. The experimental results inherently depend on the pH of the solution [27]. However, the focus here is on presenting potential mechanisms of adsorption and degradation, without specifically detailing pH-dependent effects. Two primary types of interactions electrostatic adsorption and hydrogen bonding significantly contribute to the adsorption of CEX by the nanofibers. The amine groups in the chitosan structure are may protonated (NH_3^+), while CEX molecules exist in a zwitterionic form, containing both protonated amine and carboxylate groups (COO^-). In this state, strong electrostatic attraction occurs between the NH_3^+ groups of chitosan and the COO^- groups of CEX. Additionally, hydrogen bonds form between the electron-donating groups within the CEX structure (amino, thiol, and carboxylate groups) and the functional groups of chitosan (NH_2 and OH).

Fig. 8

Fig. 9 presents the FTIR spectra of chitosan nanofibers before and after the adsorption of CEX. As illustrated, the intensities of peaks associated with amine and hydroxyl groups decreased following CEX adsorption, indicating the formation of hydrogen bonds between chitosan and CEX. Additionally, the new peaks observed at 1563 and 1716 cm^{-1} correspond to the amine and carbonyl (C=O) functional groups within the structure of CEX, confirming the adsorption of CEX molecules onto the chitosan nanofiber layer. During the adsorption process, the CEX molecules adsorbed onto chitosan are rapidly degraded through photocatalytic reactions. The BCT photocatalyst degrades pollutant molecules through a Z-scheme charge transfer mechanism [27]. Consequently, the TiO_2 and Bi_2WO_6 semiconductors, respectively, become electron-rich and hole-rich regions. The electrons in the TiO_2 conduction band either directly react with CEX or reduce the adsorbed oxygen molecules. Likewise, the holes in the Bi_2WO_6 valence band oxidize CEX molecules or the adsorbed water molecules. As a result, the mineralization of this pollutant is achieved in the presence of generated radical species.

The presentation of these results is intended solely to emphasize that, for achieving higher predictive accuracy and a more comprehensive simulation, these mechanisms should be incorporated into an advanced model in the future.

Fig. 9

6. Conclusion

This study successfully demonstrated the simulation of photocatalytic degradation of CEX pollutant in a planar microreactor using COMSOL Multiphysics. The developed model showed a strong correlation with available experimental data, confirming the accuracy and reliability of the predicted results. The effect of the geometric dimensions of the microreactor on the efficiency of pollutant degradation was investigated. It was found that reducing the depth of the microreactor from 300 to 100 μm increased the pollutant removal efficiency by 10%. Additionally, increasing the length of the microreactor from 50 to 100 mm enhanced the pollutant degradation efficiency by 15%. The calculated Damköhler number under optimal experimental conditions indicates that the photocatalytic degradation process is primarily controlled by reaction kinetics rather than the mass transfer rate. This study provides valuable insights into the impact of geometric dimensions and removal mechanisms on pollutant degradation in microreactors, and it may help future research in designing microreactors with optimal geometric sizes.

References

[1] Kirby. M, Mainuddin. M, "The impact of climate change, population growth and development on sustainable water security in Bangladesh to 2100", *Sci. Rep.* 12 (2022) 1–12. https://doi.org/10.1038/s41598-022-26807-6

[2] Qin. K, Zhao. Q, Yu. H, *et al.* "A review of bismuth-based photocatalysts for antibiotic degradation: Insight into the photocatalytic degradation performance, pathways and relevant mechanisms," *Environ. Res.*, vol. 199, no. May, p. 111360, 2021. https://doi.org/10.1016/j.envres.2021.111360

[3] Amangelsin. Y, Semenova. Y, Dadar. M, et al. "The impact of tetracycline pollution on the aquatic environment and removal strategies," *Antibiot.* 2023, Vol. 12, Page 440. 12 (2023) 440. https://doi.org/10.3390/antibiotics12030440

[4] Radwan. E.K, Abdel Ghafar. H.H, Ibrahim. M.B.M, et al. "Recent trends in treatment technologies of emerging contaminants," *Environ. Qual. Manag.* 32 (2023) 7–25. https://doi.org/10.1002/tqem.21877

[5] Al-Nuaim. M.A, Alwasiti. A.A, Shnain. Z.Y, "The photocatalytic process in the treatment of polluted water," *Chem. Pap*. 2022 772. 77 677–701. https://doi.org/10.1007/s11696-022-02468-7

[6] Padoin. N, Soares. C, "An explicit correlation for optimal TiO_2 film thickness in immobilized photocatalytic reaction systems," *Chem. Eng. J.*, 2017. vol. 310, pp. 381–388. https://doi.org/10.1016/j.cej.2016.06.013

[7] Akman. B, Aras. O, "Usability, durability and regeneration of Ag/ZnO coated microreactor for photocatalytic degradation of methylene blue," *J. Mol. Struct.* 1251 (2022) 132003. https://doi.org/10.1016/j.molstruc.2021.132003

[8] Lira. J. O. D. B, Riella. H. G, Padoin. N, et al. "Fluid dynamics and mass transfer in curved reactors: A CFD study on dean flow effects," *J. Environ. Chem. Eng.*, 2022. vol. 10, no. 5. https://doi.org/10.1016/j.jece.2022.108304

[9] Rouhani. Sand, Taghipour. F, "Modeling of UV-LED photocatalytic reactors for the degradation of gaseous volatile organic compounds (VOCs) in indoor environments," *J. Environ. Chem. Eng.*, 2022. vol. 10, no. 3, p. 107657,. https://doi.org/10.1016/j.jece.2022.107657

[10] Janczarek. M, and Kowalska. E, "Computer simulations of photocatalytic reactors," *Catalysts*, 2021. vol. 11, no. 2, pp. 1–15. https://doi.org/10.3390/catal11020198

[11] Liu. X, Zhang. J, Nielsen. K. D, et al. "Challenges and opportunities of computational fluid dynamics in water, wastewater, and stormwater treatment," *J. Environ. Eng.*, 2020. vol. 146, no. 11, pp. 1–4. https://doi.org/10.1061/(ASCE)EE.1943-7870.0001815

[12] Hasanpour. M, Motahari. S, Jing. D, et al. "Numerical modeling for the photocatalytic degradation of methyl orange from aqueous solution using cellulose/zinc oxide hybrid aerogel: comparison with experimental data," *Top. Catal.*, 2021. no. 0123456789. https://doi.org/10.1007/s11244-021-01451-y

[13] Orozco. S, Rivero. M, Suárez-Parra. R, et al. "Theoretical–experimental methodology for designing hybrid photocatalytic reactors," *Top. Catal.*, 2022. vol. 65, no. 9–12, pp. 1000–1014. https://doi.org/10.1007/s11244-022-01677-4

[14] Asgharian. M, Khoshandam. B, Mehdipourghazi. M, et al. "Photocatalytic degradation of tetracycline in a stirred tank: computational fluid dynamic modeling and data validation," *React. Kinet. Mech. Catal.*, 2021. vol. 134, no. 1, pp. 553–568. https://doi.org/10.1007/s11144-021-02062-0

[15] Corbel. S, Becheikh. N, Roques-Carmes. T, et al. "Mass transfer measurements and modeling in a microchannel photocatalytic reactor," *Chem. Eng. Res. Des.*, 2014. vol. 92, no. 4, pp. 657–662. https://doi.org/10.1016/j.cherd.2013.10.011

[16] Jayamohan. H, Smith. Y. R, L. Hansen. C, et al. "Anodized titania nanotube array microfluidic device for photocatalytic application: Experiment and simulation," *Appl. Catal. B Environ.*, 2015. vol. 174–175, pp. 167–

175. https://doi.org/10.1016/j.apcatb.2015.02.041

[17] Satuf. M. L, Macagno. J, Manassero. A, et al. “Simple method for the assessment of intrinsic kinetic constants in photocatalytic microreactors,” *Appl. Catal. B Environ.*, 2019. vol. 241, pp. 8–17. https://doi.org/10.1016/j.apcatb.2018.09.015

[18] Behineh. E. S, Solaimany Nazar. A.R, Farhadian. M, et al. “Three-dimensional simulation of microcapillary and microchannel photo reactors for organic pollutant degradation from contaminated water using computational fluid dynamics,” *Adv. Environ. Technol.*, 2019. vol. 5, no. 4, pp. 229–237. https://doi.org/10.22104/aet.2020.4036.1203

[19] Corbel. S, Donat. F, and Schneider. R, “Kinetic study of photocatalytic degradation of Ifos famide in a microchannel and simulation,” *SDRP J. Nanotechnol. Mater. Sci.*, 2019. vol. 2, no. 1, pp. 1–10.

[20] Yusuf. A, Oladipo. H, Ozer. L, *et al.*, “Modelling of a recirculating photocatalytic microreactor implementing mesoporous N-TiO_2 modified with graphene,” *Chem. Eng. J.*, 2020. vol. 391. https://doi.org/10.1016/j.cej.2019.123574

[21] Yusuf. A and Palmisano. G, “Three-dimensional CFD modelling of a photocatalytic parallel-channel microreactor,” *Chem. Eng. Sci*, 2021. vol. 229, p. 116051. https://doi.org/10.1016/j.ces.2020.116051

[22] Rabanimehr. F, Farhadian. M, Solaimany Nazar. A.R, et al. “Simulation of photocatalytic degradation of methylene blue in planar microreactor with integrated ZnO nanowires,” *J. Appl. Res. Water Wastewater*, 2021. vol. 8, no. 1, pp. 36–40. https://doi.org/10.5555/20210431393

[23] Rabanimehr. F, Farhadian. M, and Solaimany Nazar. A.R, “A high-performance microreactor integrated with chitosan/ Bi_2WO_6/CNT/TiO_2 nanofibers for adsorptive/photocatalytic removal of cephalexin from aqueous solution,” *Int. J. Biol. Macromol*, 2022. vol. 208, pp. 260–274. https://doi.org/10.1016/j.ijbiomac.2022.03.108

[24] Vilt. M.E, Ho. W.S.W, “Supported liquid membranes with strip dispersion for the recovery of cephalexin,” *Michael, Elsevier*, 2009. vol. 342, pp. 80-87. https://doi.org/10.1016/j.memsci.2009.06.026

[25] Mills. A, Wang. J, and Ollis. D. F, “Dependence of the kinetics of liquid-phase photocatalyzed reactions on oxygen concentration and light intensity,” *J. Catal*, 2006. vol. 243, no. 1, pp. 1–6. https://doi.org/10.1016/j.jcat.2006.06.025

[26] Dionysiou. D. D, Suidan. M. T, Baudin. I, et al. “Oxidation of organic contaminants in a rotating disk photocatalytic reactor: Reaction kinetics in the liquid phase and the role of mass transfer based on the dimensionless Damköhler number,” *Appl. Catal. B Environ*, 2002. vol. 38, no. 1, pp. 1–16. https://doi.org/10.1016/S0926-3373(02)00012-7

[27] Rabanimehr. F, Farhadian. M, and Solaimany Nazar. A.R, et al. “Fabrication of Z-scheme Bi_2WO_6/CNT/TiO_2 heterostructure with enhanced cephalexin photodegradation: Optimization and reaction mechanism,” *J. Mol. Liq.*, 2021. vol. 339, p. 116728. https://doi.org/10.1016/j.molliq.2021.116728

[28] Ergu. O. B, Sara. O. N, Yapici. S, et al “Pressure drop and point mass transfer in a rectangular microchannel,” *Int. Commun. Heat Mass Transf*, 2009. vol. 36, no. 6, pp. 618–623. https://doi.org/10.1016/j.icheatmasstransfer.2009.03.015

Biographies:

Mohammad Reza Abbasi is a Ph.D. candidate in department of chemical engineering at University of Isfahan. His research focuses on the treatment of pollutants using advanced oxidation processes. He has a strong interest in pollutant remediation and the simulation of treatment processes.

Fayazeh Rabbanimehr is currently the director of laboratories at Shahid Montazeri power plant in Isfahan. He received his doctorate degree in chemical engineering from University of Isfahan in 2023.

Ali Reza Solaimany Nazar is currently an associate professor in the department of chemical engineering at University of Isfahan, Iran. His research interests are mainly asphaltene and wax deposition in reservoir and transportation line, adsorption and advanced oxidation process in water and wastewater treatment.

Mehrdad Farhadian is currently a professor in the department of chemical engineering, University of Isfahan, Iran. He is a member of the Environmental Research Institute at the University of Isfahan, Iran. His main research interests include water and wastewater treatment and environmental engineering in the field of chemical engineering.

Captions of Figures and Tables

Fig. 1. (a) Picture of the assembled microreactor and (b) schematic image of the dissembled microreactor [23]

Fig. 2. The mesh scheme

Fig. 3. Comparison between model and available experimental data [23] on CEX removal in terms of residence time at inlet concentrations (a) 30 mg/L, (b) 40 mg/L, (c) 50 mg/L and (d) 60 mg/L

Fig. 4. Concentration distribution of CEX in the microreactor under optimal experimental conditions [23] (residence time 252 seconds, inlet concentration 29 mg/L, and flow rate 71 µL/min)

Fig. 5. The effect of microreactor depth on CEX pollutant removal efficiency under optimal experimental conditions [23] (volumetric flow rate 1.1905×10^{-9} m^3/s and inlet concentration 29 mg/L)

Figures:

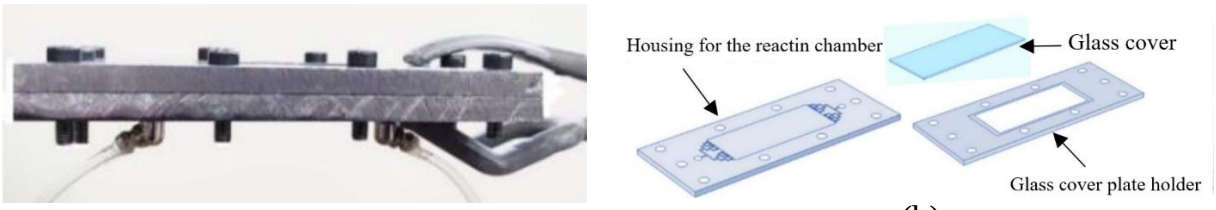

Fig. 7. (a) Picture of the assembled microreactor and (b) schematic image of the dissembled microreactor [23]

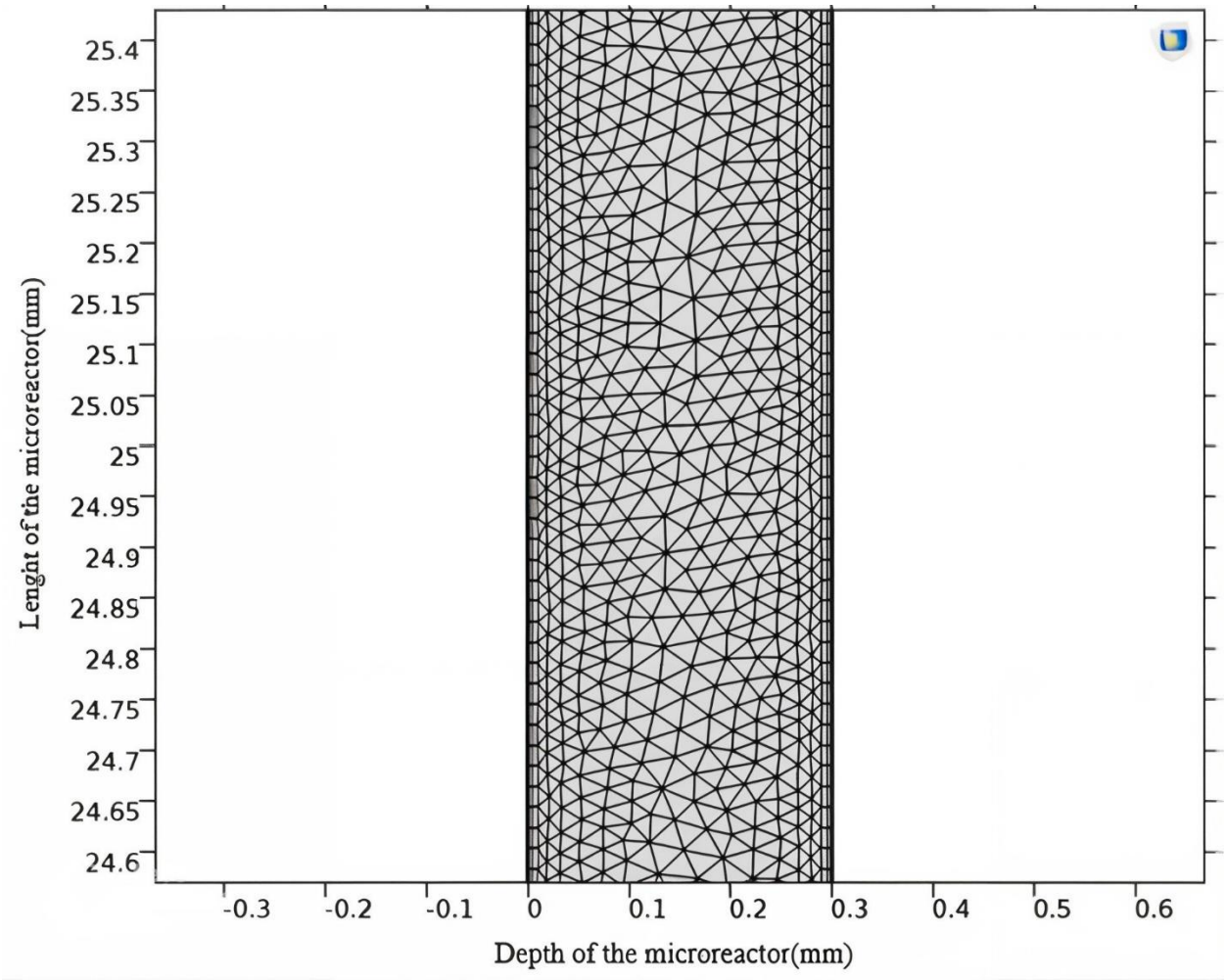

Fig. 8. The mesh scheme

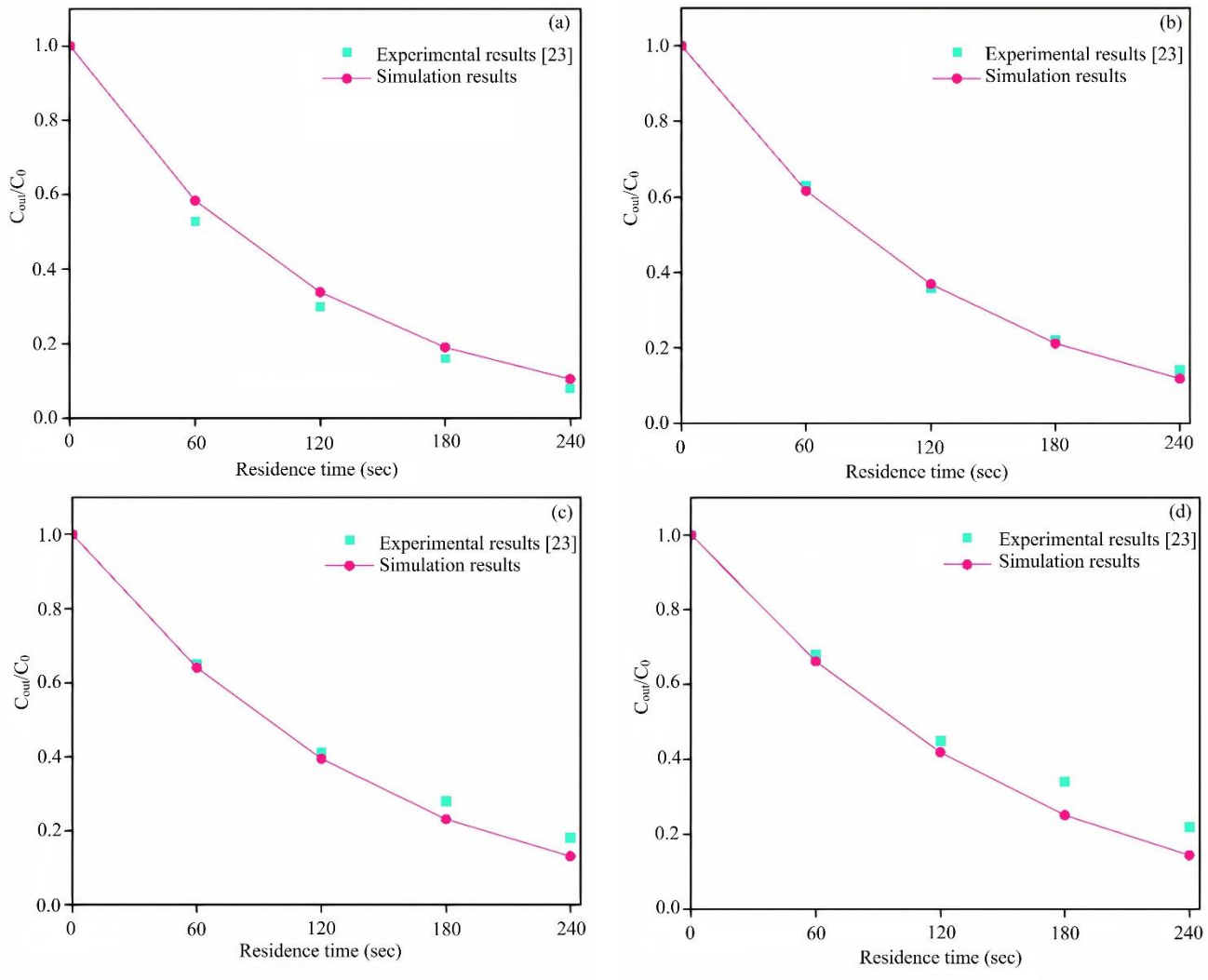

Fig. 9. Comparison between model and available experimental data [23] on CEX removal in terms of residence time at inlet concentrations (a) 30 mg/L, (b) 40 mg/L, (c) 50 mg/L and (d) 60 mg/L

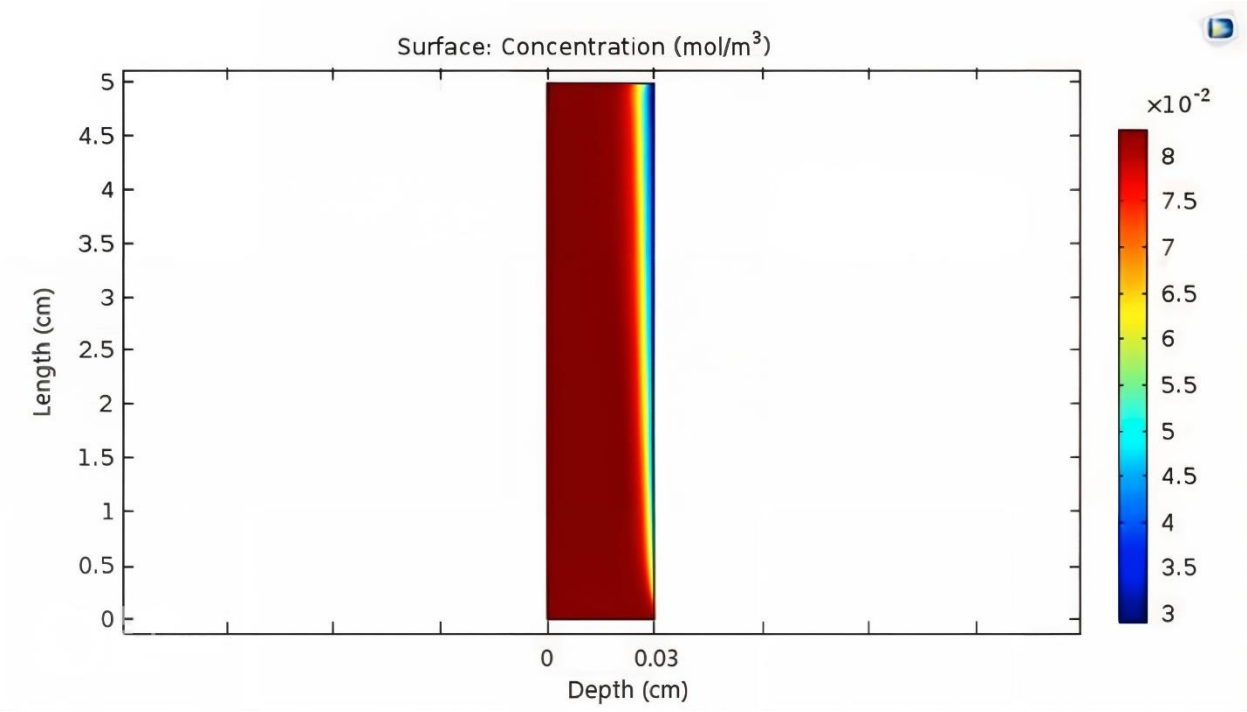

Fig. 10. Concentration distribution of CEX in the microreactor under optimal experimental conditions [23] (residence time 252 seconds, inlet concentration 29 mg/L, and flow rate 71 µL/min)

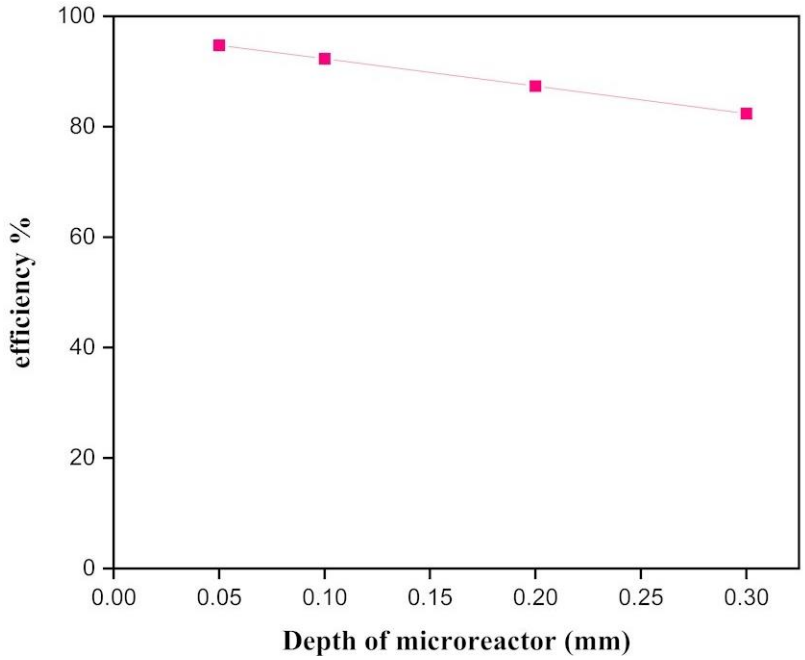

Fig. 11. The effect of microreactor depth on CEX pollutant removal efficiency under optimal experimental conditions [23] (volumetric flow rate 1.1905×10^{-9} m^3/s and inlet concentration 29 mg/L)

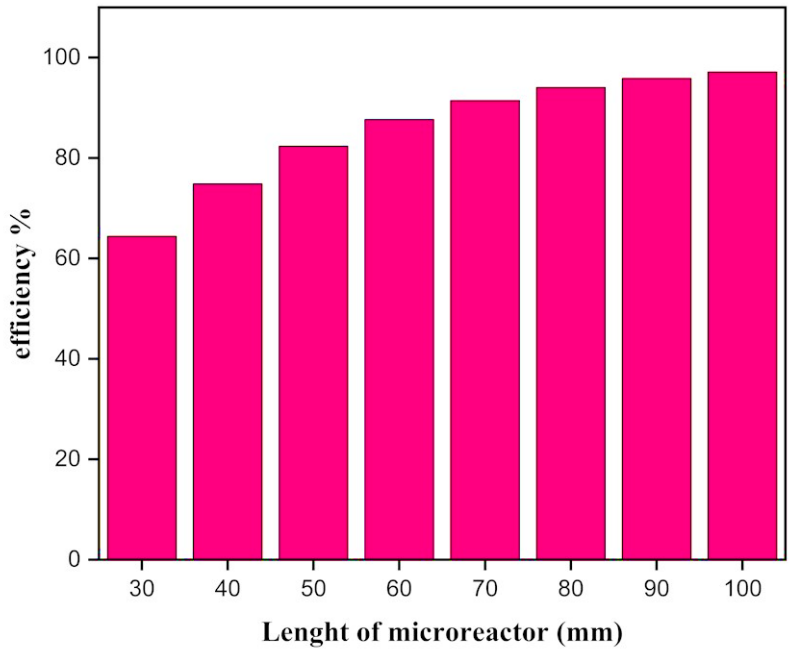

Fig. 12. The effect of microreactor length on pollutant removal efficiency under optimal experimental conditions [23] (volumetric flow rate 1.1905×10^{-9} m^3/s and inlet CEX concentration 29 mg/L)

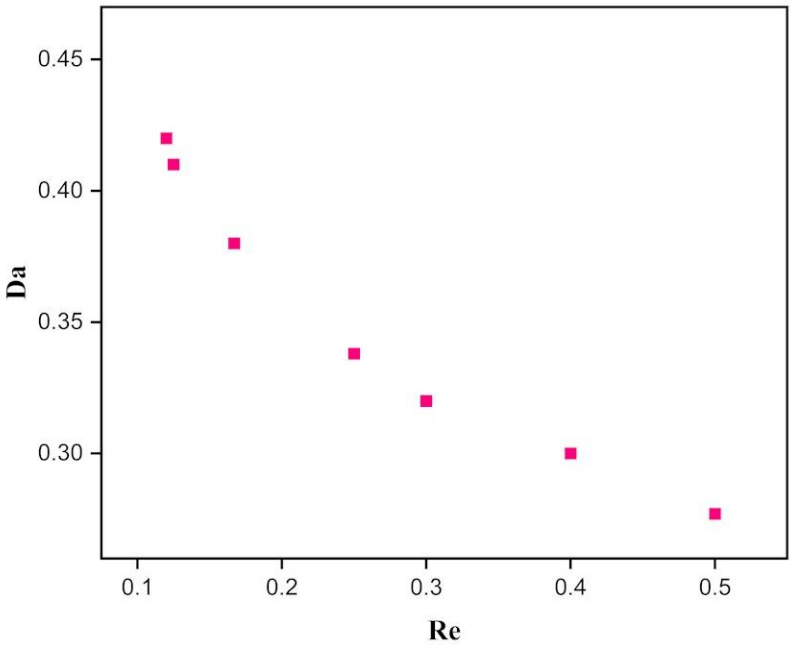

Fig. 7. The variation of the Damköhler number in the microreactor as a function of the Reynolds number, at the inlet concentration of 29 mg/L and different residence times

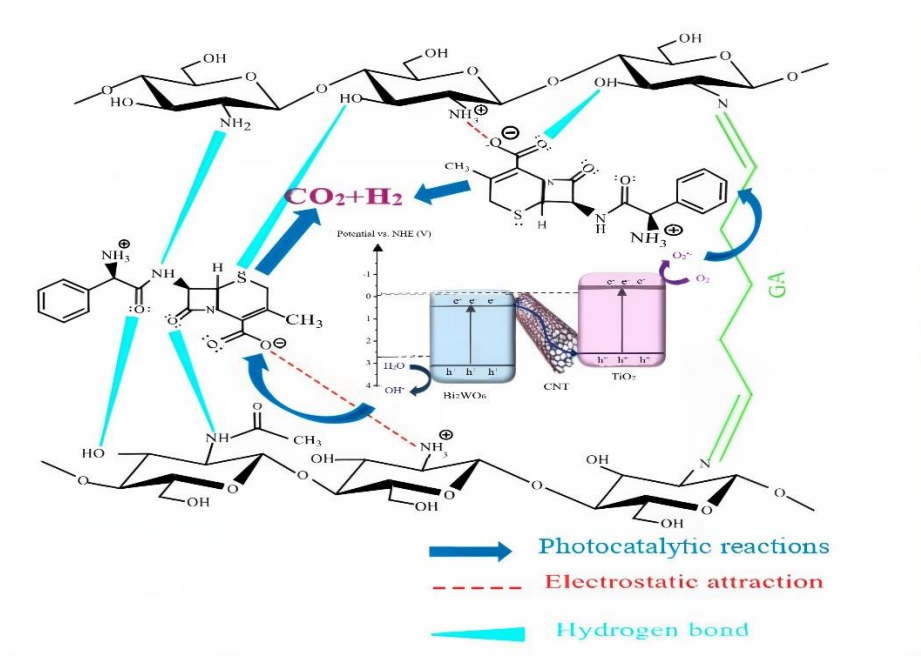

Fig. 8. Adsorption-photocatalytic mechanism for the mineralization of CEX pollutant in the presence of nanofibers BCT/CHT

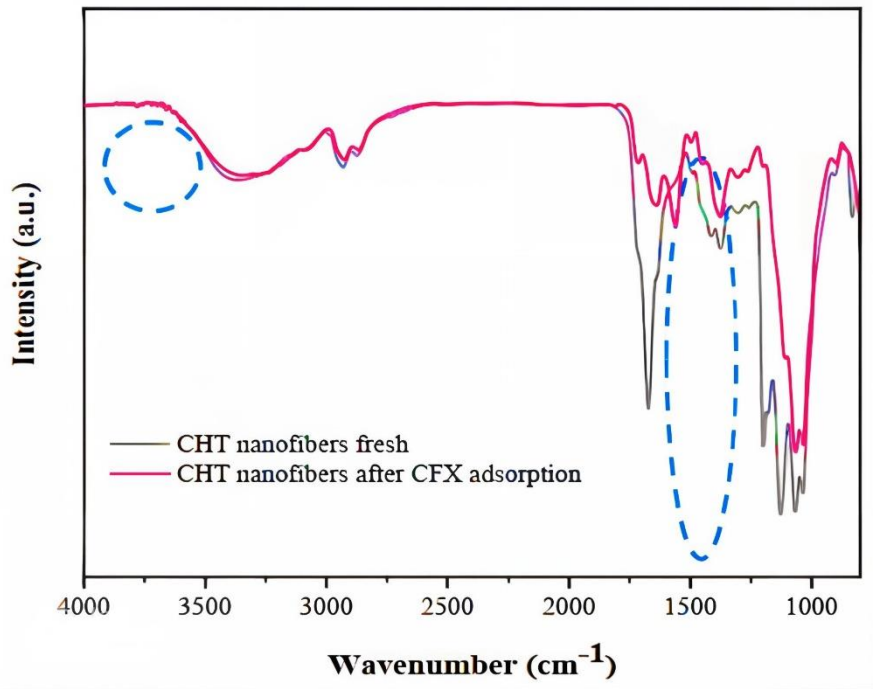

Fig. 9. FTIR spectrum of chitosan nanofibers before and after CEX adsorption

Tables

Table 1. Geometric characteristics of the planar microreactor and operating conditions [23]

Length (mm)	Width (mm)	Depth (mm)	Volume (mm^3)	specific surface area (m^{-1})	Inlet concentrations (mg/L)	Flow rates (µL/min)
50	20	0.3	300	3330	30,40,50,60	75,100,150, 300

Table 2. Mesh independence analysis under conditions of inlet concentration of 60 mg/L and residence time of 180 seconds

	Coarser mesh	Coarse mesh	Normal mesh
Number of elements	27508	49318	75672
Minimum element size (mm)	0.00232	0.00174	0.00116
Experimental C/C_0	0.34	0.34	0.34
Simulation C/C_0	0.316	0.322	0.33

Table 3. Comparison of experimental and predicted photocatalytic degradation in 2D and 3D simulations at different CEX inlet concentration

Inlet concentration of pollutant (mg/L)	Predicted efficiency in 2D simulation (%)	Predicted efficiency in 3D simulation (%)	Experimental efficiency (%) [23]
30	89	91	92
40	88	87	86
50	86	84	82
60	85	82	78

Table 4. Difference percentage between 2D and 3D simulations results

Inlet concentration of pollutant (mg/L)	Difference percentage of 2D and 3D simulations results (%)
30	2.2
40	1.15
50	2.3
60	3

Table 5. The percent of average absolute deviation at different inlet concentration of CEX

Inlet concentration of pollutant (mg/L)	ADD%
30	3.72
40	1.31
50	3.1
60	5.33